System matrix generation for angular domain tomographic reconstruction

Torres, Veronica, Li, Chengyue, Brankov, Jovan, Tichauer, Kenneth

Veronica C. Torres, Chengyue Li, Jovan G. Brankov, Kenneth M. Tichauer, "System matrix generation for angular domain tomographic reconstruction," Proc. SPIE 11229, Advanced Biomedical and Clinical Diagnostic and Surgical Guidance Systems XVIII, 112290M (21 February 2020); doi: 10.1117/12.2545999

SPIE.

Event: SPIE BiOS, 2020, San Francisco, California, United States

System matrix generation for angular domain tomographic reconstruction

Veronica C. Torres*[a], Chengyue Li[a], Jovan G. Brankov[b], Kenneth M. Tichauer[a]
[a]Department of Biomedical Engineering, Illinois Institute of Technology, 3255 S Dearborn St., Chicago, IL USA 60616; [b]Department of Electrical and Computer Engineering, Illinois Institute of Technology, 3255 S Dearborn St., Chicago, IL USA 60616

ABSTRACT

The ADEPT system is an angular domain optical projection tomography imaging system being developed to address the problem of undetected micrometastases in lymph node biopsy tissues. The relatively weak scattering nature of lymph nodes combined with a very low numerical aperture enables the approximation of straight-line projections that can be reconstructed into images simply with filtered back-projection (FBP). This was demonstrated in previous work where 0.2 mm diameter inclusions were detected in ~1 cm diameter lymph nodes; and while FBP was sufficient, the Radon transform is not a true representation of the imaging system. To investigate the degree of improvement that a more complex reconstruction algorithm could provide, a Monte Carlo based system matrix was generated and used to solve the inverse problem. Simulated phantoms were used to test this, and results revealed greater detection sensitivity at the periphery of samples. Such findings lend guidance in the ongoing design of the ADEPT system and so more robust evaluation of the reliability of the system matrix will be implemented in future work.

Keywords: angular domain, optical projection tomography, lymph node, tomographic reconstruction, system matrix

1. INTRODUCTION

Optical projection tomography (OPT) has been used extensively for three-dimensional (3-D) visualization of structures within biological specimens. For instance, high resolution imaging of individual islets, microvasculature, and gene expression from whole rodent organs, embryos, and xenograft tumors have been achieved[1-3]. One application where this capability for virtual sectioning can be especially useful is in the evaluation of sentinel lymph node biopsies, where the current standard for pathological assessment – results of which affect cancer treatment decisions and consequently patient prognosis – has high rates of false negatives (missed metastases within the tissue). This occurs largely because of the time consuming nature of the process, and as such, less than 1% of the tissue volume is actually evaluated.[4] With the possibility for rapid, whole node visualization, OPT offers a promising alternative solution.

Currently, an angular domain early photon tomography (ADEPT) imaging system is being developed to address this challenge.[5,6,7] While conventional OPT requires optical clearing of the tissue to enable straight-line projections and therefore, simple back-projection reconstruction algorithms, the ADEPT method makes use of the low scattering properties of lymph nodes and angular domain imaging to facilitate more parallel rays. By reducing the detector angle of acceptance, only the early and straightest traveling photons are collected. Although greater levels of scatter rejection can theoretically provide enhanced spatial resolution, there is a tradeoff with the number of photons detected. Through simulation[5,7], it was demonstrated that for the particular application of lymph node assessment (3-6 mm diameter samples with low scattering optical properties), strict angular restriction (NA = 0.005) and filtered back-projection (FBP) reconstruction were sufficient to detect and localize 200 μm "micrometastases" – the smallest clinically relevant. Based on these simulations, a prototype system was developed following the same configuration (Fig. 1). Experimentation with the system and fluorescent inclusions in porcine lymph nodes revealed similar promising findings[6].

While FBP can provide adequate results, it is of interest to explore other methods of reconstruction to determine the degree of improvement that more complex algorithms can offer. In addition, inherent to OPT, is a limited depth of focus. That is, depending on where the focal plane is positioned, different parts of each image contain focused and out-of-focus data; and although angular domain scatter rejection aids in reducing the numerical aperture, thereby increasing the depth of focus, it is not an idealized parallel beam system.[3] In this work, construction of a system matrix was investigated where Monte Carlo simulations were used to model the behavior of the imaging system. The aim in generating such system matrices is

Advanced Biomedical and Clinical Diagnostic and Surgical Guidance Systems XVIII, edited by Anita Mahadevan-Jansen
Proc. of SPIE Vol. 11229, 112290M · © 2020 SPIE · CCC code: 1605-7422/20/$21 · doi: 10.1117/12.2545999

to be able to compare reconstruction performance to push the limits of spatial resolution, and to help in the design of the imaging system.

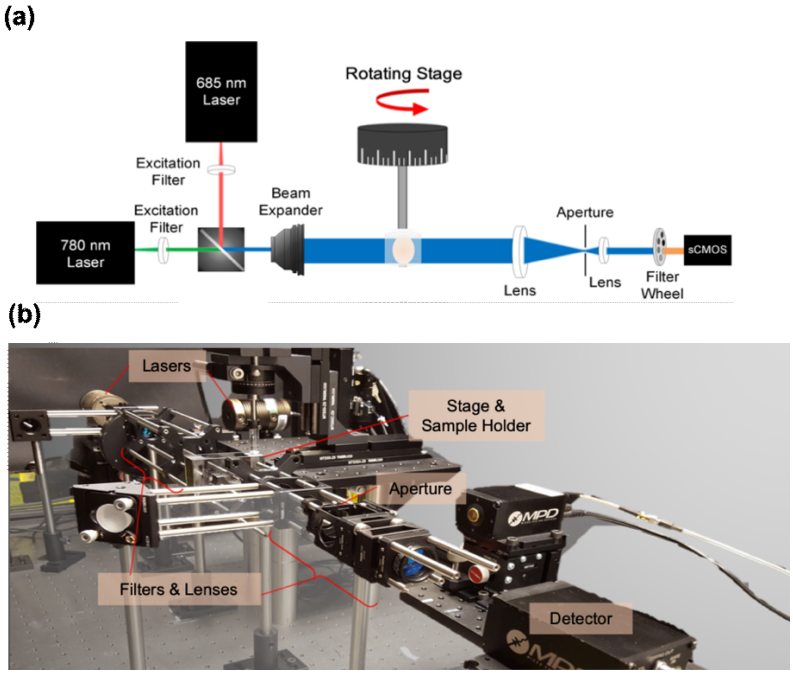

Figure 1. (a) Schematic of the angular domain early photon tomography (ADEPT) system. Angular domain imaging is achieved via restriction of the aperture (adjustable iris diaphragm). (b) System prototype.

2. METHODS

2.1 Tomographic reconstruction problem as a system of linear equations

The inverse problem of tomographic image reconstruction can be modeled as a system of linear equations:

$$\vec{g} = \boldsymbol{H}\vec{f} \tag{1}$$

where $\vec{g}$ is an M-dimensional column vector representing the 2D measured image data; $\vec{f}$ is an N= (n x n)-dimensional column vector of the voxelized object; and $\boldsymbol{H}$ is an MxN system matrix that transforms the object data to image data. The measured data, $\vec{g}$, is made up of m detectors for k different angles, such that $M = m$ x k. Elements of the system matrix, h_{ij}, each represent the contribution of the voxel j to pixel i Thus, each row in $\boldsymbol{H}$ is the contribution of all voxels to a given pixel, and each column is the vectorized 2D image corresponding to a single voxel. The value or weight of each element is based on several aspects of the imaging system, which include source illumination geometry, detector response, aberrations from optical components, sample properties (geometry and optical scattering, attenuation, etc.) and specifications of the actual image acquisition.

2.2 Monte Carlo simulations

Source and detector sensitivity profiles were generated from Monte Carlo (MC) simulated data using the open-source MCmatlab[8] program. Simulations were structured to match the configuration of the ADEPT system: the source was 780 nm wide-field gaussian beam illumination focused at half the sample depth such that the entire sample was illuminated [Fig. 2(a)]; and single detectors were modeled as pencil beams with divergence set to meet a strict NA of 0.005 [Fig. 2(b)]. As a preliminary test, samples were modeled as 1 cm^3 cuboids with lymph node matching optical properties (μ_a = 0.3 cm^{-1}, μ_s = 43 cm^{-1}, g = 0.92, n = 1.4). The size of the object was 101x101x101 voxels. Source, and every detector element (m = 101) simulations were run for 10 min each, with $3.4x10^7$ and $2.7x10^7$ photons launched, respectively, resulting in 17 h of simulation time. Although 3D photon propagation through the sample was modeled and volumetric reconstruction is possible, 2D analysis was carried out for simplicity.

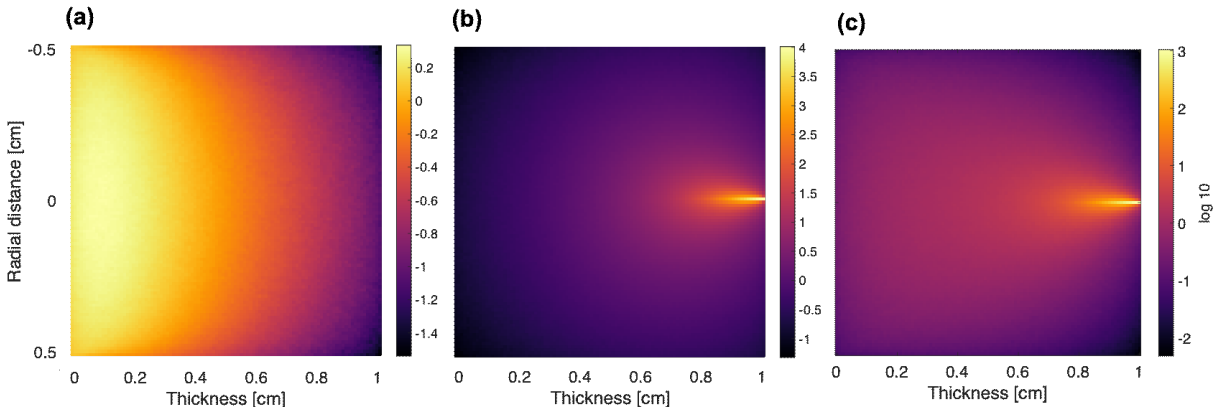

Figure 2. Monte Carlo simulations to construct ADEPT system sensitivity profiles. (a) Source sensitivity profile: gaussian beam widefield illumination. (b) Representative detector sensitivity profile: beam with divergence set to model strict angular restriction. (c) Representative source-detector pair sensitivity profile.

2.3 System matrix generation

The imaging system was modeled to follow light traveling from left to right: from the source, through the sample and then collection at the detector [Fig 1(a)]. For 2D reconstruction, a single slice (middle of the object, z = 50) in the x-y plane, parallel to the optical axis and perpendicular to the axis of rotation was used. Source and detector sensitivity profiles were multiplied on an element-wise basis to construct individual source-detector pair probabilities [Fig. 2(c)]. Each source-detector pair was then rotated over 360˚ in 1˚ intervals. Matrices were padded so as not to lose any information during rotation. Elements of each of these sensitivity profiles were vectorized and ordered to generate the total system sensitivity matrix, following $\boldsymbol{H}$ = [k angles x m detectors, n x n pixels]. Here, the size of $\boldsymbol{H}$ was 36,360x10,201.

3. RESULTS AND DISCUSSION

To test the produced system matrix, 2D single point illumination phantoms were constructed, and image data was generated by transforming the phantom object via $\boldsymbol{H}$. A non-optimized iterative reconstruction algorithm[9] using the resultant transform matrix was used and compared to image reconstructions with simple FBP. Because construction of $\boldsymbol{H}$ can become very large and computationally expensive, and to permit quick investigation of different imaging system configurations, the system matrices were scaled down to 13 detectors and pixels each. For iterative reconstruction, a matrix of ones was used as the first guess and filtered backprojection was performed using the built-in `iradon` MATLAB function. The results are shown in Figure 3. As expected, it can be seen that reconstruction using the generated system matrix improved with progressive iterations. It should also be noted that performance improved as the illuminated object moved from the center towards the edges. In the first row, the object was located directly in the middle at (7,7), and after 20 iterations, the actual illuminated voxel was constructed but there was obvious error surrounding the point. As the object moved to the right with coordinates (9,7), shown in the second row, the expected point was again captured; however, this time there was much less blur around it. Moving further to the periphery at (10,3), the algorithm appeared to perform best with only the single point being reconstructed. Contrary to the results using the system matrix, FBP outperformed the iterative algorithm when the object was closer to the center. Interestingly, the image reconstructions from solving the inverse problem with the generated $\boldsymbol{H}$, produced circular structures. This may be explained by looking at the source-detector sensitivity profile [Fig. 2(c)], where the strict acceptance angle of the single detector restricts sensitivity to a limited distance. Rotating this around 360˚, the result is a circle with probability of detection orders of magnitude higher for a very small depth near the periphery compared to the rest of the internal sample. This is also likely the reason for enhanced performance of reconstruction for objects located away from the center.

Findings such as this, demonstrate the utility in exploring sensitivity profiles of the imaging system being developed. Larger numerical apertures can be tested to increase the probability of detection and reduce the ring-like sensitivity. In addition, more accurate modeling of the sample and the actual image acquisition process can be carried out. For instance, lymph nodes are generally ellipsoid in shape, and the procedure for ADEPT imaging involves embedding the lymph node tissue in cylindrical transparent agarose gel, which is then submerged in a water bath made of acrylic. Whereas the system matrix above was generated from a “lymph node” cuboid, matrices can be developed that better represent the system.

Figure 4 illustrates an example where a lymph node is modeled as an ellipsoid within a water bath. With this, a similar procedure of MC simulation to produce sensitivity profiles and a system matrix as described above can be employed.

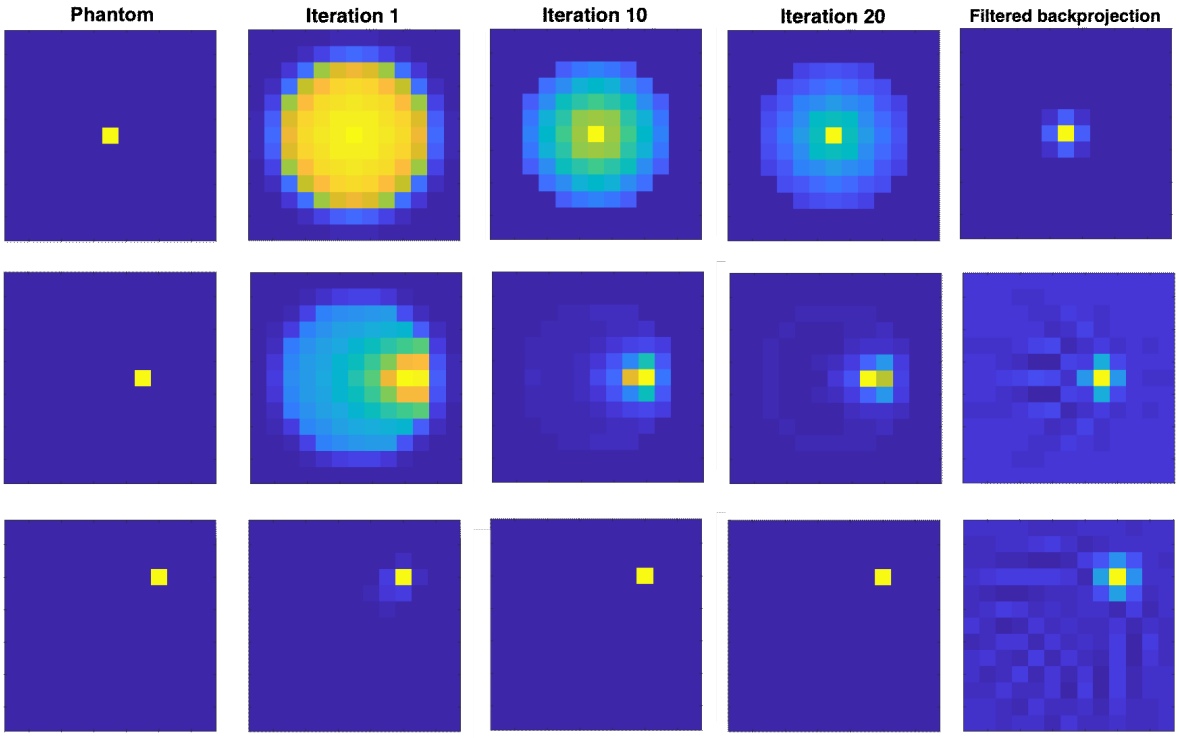

Figure 3. Test phantom reconstructions. First column: 13x13 pixel object phantoms with single illumination points at (7,7), (9,7) and (10,3) for rows one through three, respectively. Middle three columns: Reconstructions for multiple iterations using the generated system matrix **H.** Last column: Filtered backprojection reconstructions for comparison.

As a first investigation in characterizing the ADEPT imager into a system matrix, the results here are preliminary. Image reconstruction was simply evaluated qualitatively; however, future work will quantify performance with metrics of mean square error and signal to noise ratio in comparing the reference and reconstructed images. Reliability of the system matrix and MC-generated sensitivity profiles used as inputs will also be characterized by looking at convergence of the matrix elements.

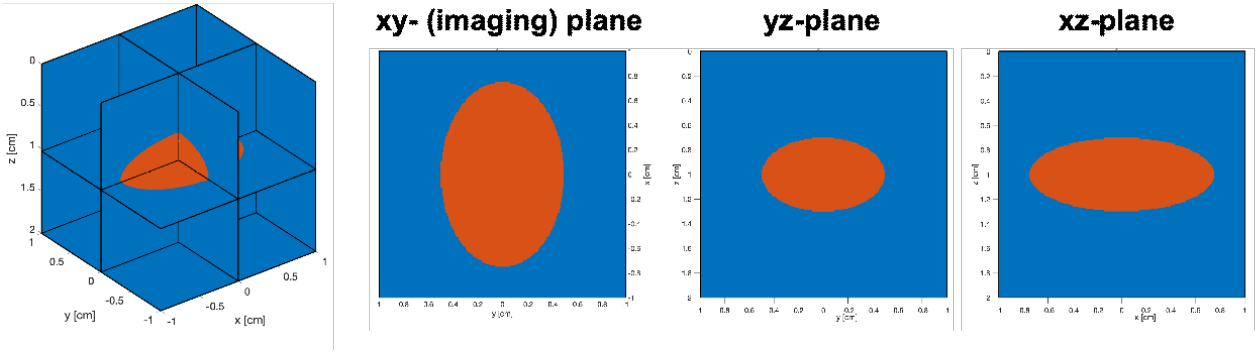

Figure 4. Sample geometry of a lymph node (orange) in a water bath (blue) for Monte Carlo simulations, each having appropriate optical properties.

4. CONCLUSION

The work presented here demonstrated the feasibility of a Monte Carlo generated system matrix for tomographic reconstruction. While the model used here was simplified, the same approach can be extended to more complex systems to account for specifics of the imaging system (e.g. optical aberrations, detector response). The strict angular domain setup of the ADEPT imager currently being developed was modeled, and the results provided insight as to how the setup affects image reconstruction, which can then be used to guide the design of the system.

REFERENCES

[1] Alanentalo T., Asayesh A., Morrison H., Lorén C.E., Holmberg D., Sharpe J., and Ahlgren U., "Tomographic molecular imaging and 3D quantification within adult mouse organs," Nature methods, vol. 4, no. 1, pp. 31-33, (2007).

[2] Eriksson, A.U., Svensson, C., Hörnblad, A., Cheddad, A., Kostromina, E., Eriksson, M., Norlin, N., Pileggi, A., Sharpe, J., Georgsson, F., Alanentalo, T., Ahlgren, U., "Near Infrared Optical Projection Tomography for Assessments of β-cell Mass Distribution in Diabetes Research," J. Vis. Exp. (71), e50238, doi:10.3791/50238 (2013).

[3] Sharpe J., "Optical Projection Tomography," Annu. Rev. Biomed. Eng. 2004. 6:209–28 doi: 10.1146/annurev.bioeng.6.040803.140210, (2004).

[4] Weaver, D.L., "Pathology evaluation of sentinel lymph nodes in breast cancer: protocol recommendations and rationale," Modern pathology: an official journal of the United States and Canadian Academy of Pathology, Inc. 23 Suppl 2, S26-32, (2010).

[5] Sinha, L., Massanes, F., Torres, V.C., Li, C., Tichauer, K.M., and Brankov, J.G., "Comparison of early-photon and angular-domain scatter rejection in mesoscopic optical imaging: a simulation study," Biomedical Optics Express, 10, 747-760, (2019).

[6] Torres, V.C., Li, C., He,Y., Sinha, L., Papavasiliou, G., Sattar, H.A., Brankov, J.G., and TIchauer K.M., "Angular restriction fluorescence optical projection tomography to localize micrometastases in lymph nodes," JBO Letters, 24(11), 110501, (2019).

[7] Torres, V.C., Sinha, L., Tichauer, K.M., Brankov, J.G., "Excised Whole Lymph Node Imaging for Cancer Staging with Angular Restriction Dual Fluorescent Optical Projection Tomography," IEEE 16th ISBI (2019).

[8] Marti, D., Aasbjerg, R.N., Andersen, P.E., Hansen, A.K., "MCmatlab: an open-source, user-friendly, MATLAB-integrated three-dimensional Monte Carlo light transport solver with heat diffusion and tissue damage," Journal of Biomedical Optics, 23(12), 121622 (2018).

[9] Lalush, D.S., and Wernick, M.N., Iterative Image Reconstruction. Emission Tomography, 443–472, (2004).